IOSR Journal of Applied Chemistry (IOSR-JAC)
e-ISSN: 2278-5736.Volume 16, Issue 5 Ser. I (May 2023), PP 04-19
www.iosrjournals.org

Inhibition Of Aluminium Corrosion In 1M Hydrochloric Acid By Three Organic Molecules (Benzoïc Acid, Acid 3-Chlorobenzoïc, Acid 3-Phenylthiobenzoïc): Adsorption, Thermodynamics, DFT, PAC And Linear QSPR.

Bamba Amara[1], Koffi Aphouët Aurélie[1], Diabaté Donourou[2], Niamien Paulin Marius[1]
[1]*Université Félix Houphouët Boigny, 22 BP 582, Abidjan 22, Côte d'Ivoire.*
[2]*Université Péléforo gon Coulibaly, BP 1328 Korhogo, Côte d'Ivoire*

Abstract
*Aluminium inhibition was investigated in 1M HCl medium by three organic molecules : benzoïc acid (**BA**), acid 3-chlorobenzoïc (**A3CB**) and acid 3-phenylthiobenzoïc (**A3PTB**). It has been observed that the corrosion inhibition efficiency IE (%) increases with increasing concentration of each of these molecules but decreases with increasing temperature. The experimental results were fitted to adsorption models as Langmuir, El-Awady, Flory Huggins… Tough, the Langmuir adsorption is the best, it can't be applied rigorously. The Villamil isotherm was therefore used. The Adejo-Ekwenchi isotherm was used to assess to the adsorption type. Thermodynamic adsorption and activation functions have been determined and examined. We also studied the influence of the solvent on the corrosion inhibition. We used Molinspiration software and DFT to determine molecular descriptors and finally PAC and QSPR method to establish a mathematical relationship between inhibition efficiency and parameters as energy gap (ΔE), molecular hydrophobicity (LogP) and E_{HOMO} (highest occupied molecular orbital).*

Key-words : *Aluminium, corrosion inhibition, adsorption isotherms, thermodynamic functions, Molinspiration, DFT, PAC, QSPR method.*

Date of Submission: 02-05-2023 Date of Acceptance: 12-05-2023

I. Introduction

Aluminium [1] is the most abundant metal in the earth's crust. It is solid at room temperature and has silver-colored in appearance and it is relatively lightweight compared to many other metals such as steel. Aluminium is commonly alloyed with other elements to increase its mechanical properties. It is preferred over steel in some applications due to its lower density, better machinability and superior corrosion resistance due to its protective oxide layer. The good performance [2] of aluminium in corrosive environment is due to the passivity produced by this protective oxide film.

Aluminum is also an excellent conductor of electricity. It is an amphoteric metal and can react with both chemically acidic and basic substances. Oxygen influences the corrosion of aluminium and accelerates the corrosion process. The attack increases in high concentrations of dissolved oxygen, especially [3-5] in acidic solutions.

There are many strategies to combat metal corrosion : chemical passivation (nitrites, chromates, zinc, molybdate…), precipitation inhibitors (sodium silicate), adsorption inhibitors (organic molecules containing heteroatoms).

Nowadays [6,7], the use of adsorption inhibitors is encouraged because of the non-toxicity of organic molecules for human beings and animal and for our environment. It is with this mind that we studied the behaviour of the three molecules : benzoïc acid and two of its derivatives (acid 3-chlorobenzoïc and acid 3-phenylthiobenzoïc).

The purpose of this work is to get information on the adsorption of the molecules onto the metal and to obtain the molecular descriptors values in order to better understand the inhibition mechanism. Therefore, the work uses the gravimetric (weight loss) method and Density Functional Theory (DFT) to access to corrosion inhibition efficiencies and molecular descriptors (E_{HOMO}, E_{LUMO}, ΔE, μ…). PCA (Principal Component Analysis) and Quantitative Structure Property Relationship (QSPR) methods were then used to get other informations on the behaviour of the studied molecules against the metal corrosion.

II. Experimental Method

Molecules

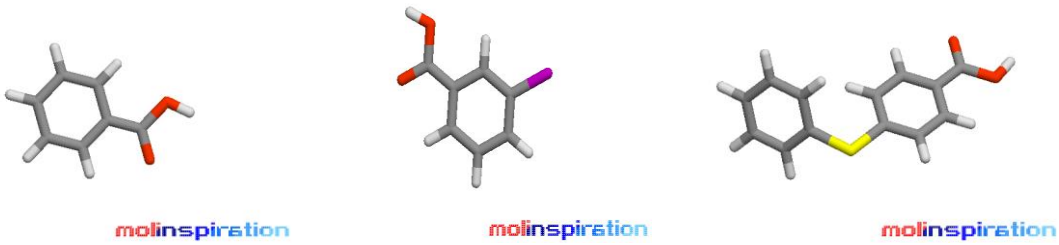

BA **A3CB** **A3PTB**

Figure 1 : Name (abbreviation) and representation of the investigated molecules

Weight loss measurement

The mass loss method [8-10] is probably the most widely used method of inhibition assessment. The aluminium samples were weighed accurately, triplicately with a balance with a sensitivity of ± 0.1mg. They were then immersed in the corrosive medium (50 mL, 1M HCl, blank) and in the blank, at different concentrations (10^{-5} to 5.10^{-4}M) of the molecules kept at 298 to 323K in a thermostat bath for one hour. Afterwards, the samples were removed from the agressive solution, throughly washed with distilled water, dried and reweighed. Each test was carried three times and the mean value of the weight loss measurement was taken into account. The corrosion rate (W) and the inhibition efficiency IE (%) were given by the equations below :

$$W = \frac{m_1 - m_2}{St} \quad (1)$$

$$IE(\%) = \frac{W_0 - W}{W_0} \times 100 \quad (2)$$

Where m_1 and m_2 are respectively the mass before and after immersion in the test solution. The immersion time is t(h), while W_0 and W are respectively the corrosion rate in the absence and presence of the studied molecules. S is the surface area of the samples in cm^2.

Quantum Chemical calculations

In order to determine a relationship between the inhibition efficiency and the molecular structure of the studied molecules, quantum chemical calculations based on DFT [11] have been performed using Gaussian 16 [12]. The hybrid density functional B3LYP exchange correlation functional, a combination of Becke three parameters [13] with the 6-311G (d, p) basis set [14] were used for the calculations of the following molecular parameters: the energy of the highest occupy molecular orbital (E_{HOMO}), the energy of the lowest inoccupied molecular orbital (E_{LUMO}), the energy gap (ΔE) and the dipole moment μ.

Global reactivity parameters

According to Parr et al. [15], the chemical potential μ_P is linked to the electronegativity χ by the equation below :

$$\mu_P = \left(\frac{\partial E}{\partial N}\right)_{v(r)} = -\chi \quad (3)$$

Where μ_P is the electronic chemical potential, E is the total energy, N is the number of electrons and v(r), the external potential of the system.

The ionization potential (I) and the electron affinity (A) of the molecules are given according to Koopman's theorem [16] :

$$I = -E_{HOMO} \quad (4)$$

$$A = -E_{LUMO} \quad (5)$$

The global reactivity descriptors [17-19] which are given with regards to finite-difference approximation are:

- The electronegativity χ [17] which is linked to the power of an atom or group of atoms to attrack electrons towards itself :

$$\chi = \frac{1}{2}(I + A) \quad (6)$$

- The chemical hardness η [18] which expresses the resistance of an atom to charge transfer :

$$\eta = \frac{1}{2}(I - A) \quad (7)$$

- The chemical softness σ [19] which measures the capacity of an atom or a group of atoms to receive electrons :

$$\sigma = \frac{1}{\eta} = \frac{2}{I - A} \quad (8)$$

When two systems, Al and an organic molecule are brought together, electrons flows from the part of lower electronegativity to that of higher electronegativity until the chemical potential are equal. The number of tranferred electrons ΔN [20] is given by the following equation :

$$\Delta N = \frac{\chi_{Al}-\chi_{inh}}{2(\eta_{Al}+\eta_{inh})} = \frac{\phi_{Al}-\chi_{inh}}{2\eta_{inh}} \quad (9)$$

Where (χ_{Al}, η_{Al}) and (χ_{inh}, η_{inh}) are respectively the electronegativity of the aluminium and oh the molecule. In this study, we use the value of $\phi_{Al} = 4.28\ eV$ [21] and $\eta_{Al} = 0$ [22] for the computation of number of the transferred electrons.

The global electrophilicity index ω [23] which measures the stabiliation in energy when the system acquires an additional electronique charge ΔN from the environment is given by the equation below :

$$\omega = \frac{\mu_P^2}{2\eta} = \frac{\chi^2}{2\eta} = \frac{(I+A)^2}{4(I-A)} \quad (10)$$

Local reactivity parameters

In order to identify the most reactive sites in a molecule, Fukui functions are used. The expression of these functions [24, 25] is commonly given by :

$$f(\vec{r}) = \left(\frac{\partial\rho(\vec{r})}{\partial N}\right)_{v(r)} \quad (11)$$

Where $\rho(\vec{r})$, N and $v(r)$ are respectively electronic density, number of electrons and external potential exerted by the nucleus.

The Yang and Mortier procedure [26] based on the finite difference method leads to the condensed Fukui functions expressed by the equations below :

$$f_k^+ = q_k(N+1) - q_k(N) \quad (12)$$

$$f_k^- = q_k(N) - q_k(N-1) \quad (13)$$

Where q_k is the electronic population of atom k in the molecule. The functions f_k^+ and f_k^- are respectively related to nucleophilic and electrophilic attacks.

Although Fukui function can reveals nucleophilic and electrophilic regions in a molecule, the dual descriptor [27, 28] is able to unambiguously expose truly nucleophilic and electrophilic regions. So, the dual descriptor can be considered as the best descriptor to measure local reactivity. This descriptor is given by :

$$\Delta f_k(r) = f_k^+ - f_k^- \quad (14)$$

Principal Component Analysis (PCA), Quantitative Structure Property Relationship(QSPR)

Principal Component Analysis

Principal Component Analysis (PCA) [29, 30] is a multivariate data analysis that converts multiple variables into a few comprehensive variables and maintains a large amount of information from the original multiple variables. PCA, in QSPR study, analyzes a data matrix in which molecules are described by several quantitative parameters interrelated. PCA [31] is widely used in the comprehensive evaluation of multiple indicators (variables) to eliminate the correlation between evaluation indicators and help find objectively the main influencing parameters.

Linear QSPR methods

After selection of sets of descriptors, multiple linear regressions were employed to develop models with the following forms :

$$EI(\%) = \boldsymbol{A}x_j + \boldsymbol{B}x_k + \boldsymbol{D}x_l + \text{Res} \quad (15)$$

Where x_j, x_k and x_l are components of a set of three parameters whereas Res is the residual.

III. Results and discussion

Weight loss experiments

In Figure 2, the inhibition efficiency of the three molecules are represented versus their concentration for different temperatures.

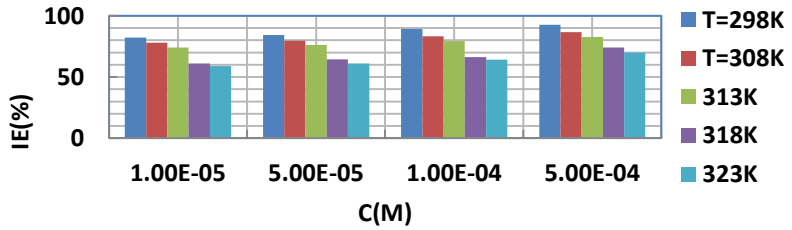

(a) : Benzoïc acid (**BA**)

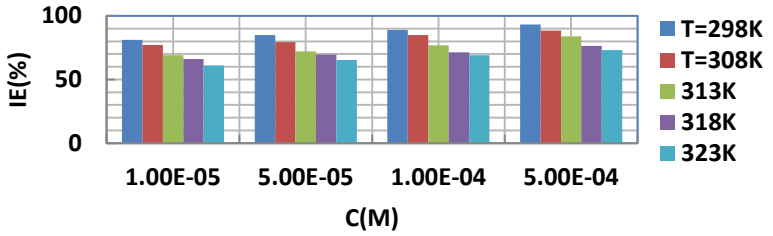

(b): Acid 3-Chlorobenzoïc (**A3CB**)

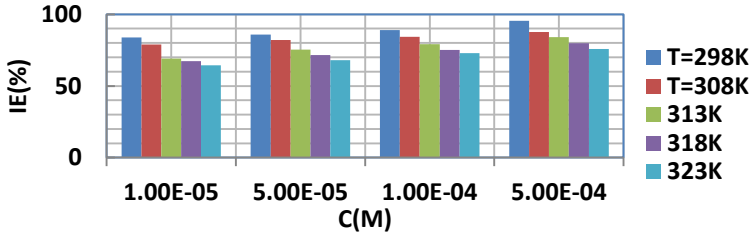

(c): Acid 3-Phenylthibenzoïc (**A3PTB**)

Figure 2 : Evolution of IE(%) versus concentration for different temperatures

Observing this figure, one can see that the three molecules have the same behaviour. their inhibition efficiency increases with increasing concentration but decreases when the temperature increases :

- **BA** : T=298K, IE(%) = 83.83 for 10^{-5}M and 95.52% for 10^{-4}M
  T=323K, IE(%) = 58.88 for 10^{-5}M and 69.91% for 10^{-4}M
- **A3CB** : T=298K, IE(%) = 81.16 for 10^{-5}M and 93.27% for 10^{-4}M
  T=323K, IE(%) = 61.06 for 10^{-5}M and 73.14% for 10^{-4}M
- **A3PTB** T=298K, IE(%) = 83.83 for 10^{-5}M and 95.52% for 10^{-4}M
  T=323K, IE(%) = 64.36 for 10^{-5}M and 75.74% for 10^{-4}M

Adsorption isotherms and Thermodynamic parameters

Metal corrosion inhibition is a surface phenomenon that may involved the adsorption of organic molecules to the metal surface in an electrolytic solution. The molecules adsorbed onto the metal surface, replacing the H_2O molecules at the metal/solution interface. The inhibition efficiency is linked to the degree of metal surface coverage. In our case, the Langmuir adsorption isotherm (Figure 3) seems to be the best model :

$$\frac{C_{inh}}{\theta} = \frac{1}{K_{ads}} + C_{inh} \qquad (16)$$

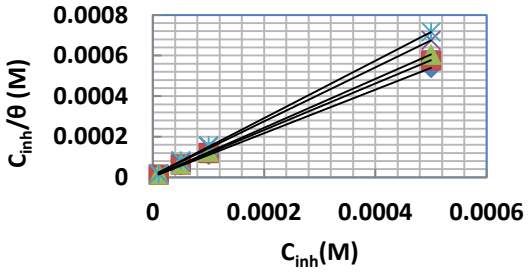

(a) BA

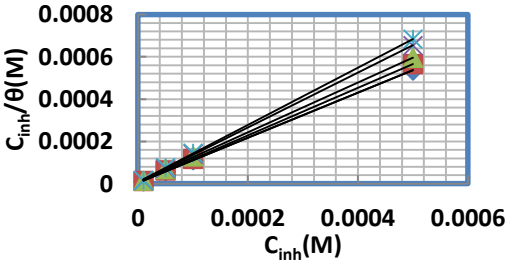

(b) A3CB

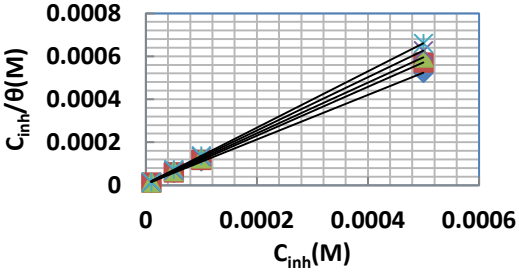

(c) A3PTB

Figure 3 : Languir adsorption curves

All the parameters linked to this isotherm are included in Table 1.

Table 1 : Langmuir isotherm parameters

Inhibitor	T(K)	K_{ads} (M^{-1})	Slope	R^2	Intercept
BA	298	52631.6	1.0121	0.9954	0.0190
	308	40000.0	1.0602	0.9905	0.0250
	313	35714.3	1.1437	0.9901	0.0280
	318	33670.0	1.1792	0.9909	0.0297
	323	32467.5	1.0168	0.9908	0.0308
B3CB	298	44642.9	1.0397	0.9934	0.0224
	308	34843.2	1.1310	0.9903	0.0287
	313	31847.1	1.1906	0.9921	0.0314
	318	29154.5	1.2792	0.9922	0.0343
	323	28571.4	1.3000	0.9924	0.0350
B3PTB	298	44247.8	1.1589	0.9953	0.0226
	308	34965.3	1.1649	0.9914	0.0286
	313	33444.8	1.2329	0.9912	0.0299
	318	28901.7	1.3234	0.9909	0.0346
	323	27472.5	1.3356	0.9911	0.0364

The determination coefficient (R^2) values of Langmuir isotherm are near the unity ; however, the slopes of the curves are different from the unity due [32, 33] to the interactions between the adsorbed species. So, the Langmuir adsorption isotherm can't be rigorously applied ; it is replaced by the modified Langmuir isotherm called Villamil isotherm which is based on the following equation :

$$\frac{C_{inh}}{\theta} = \frac{n}{K_{ads}} + C_{inh} \qquad (17)$$

Where n is the correction factor deduced from the slopes.

The values of standard free energy (ΔG^0_{ads}) of adsorption were derived from the adsorption equilibrium constant (K_{ads}) according to the following equation :

$$\Delta G^0_{ads} = -RTLn(55.5 \times K_{ads}) \qquad (18)$$

The other adsorption thermodynamic functions, change in adsorption enthalpy (ΔH^0_{ads}) and change in adsorption entropy (ΔS^0_{ads}) are deduced from the equation below :

$$\Delta G^0_{ads} = \Delta H^0_{ads} - T\Delta S^0_{ads} \qquad (19)$$

The curves are given in Figure 4.

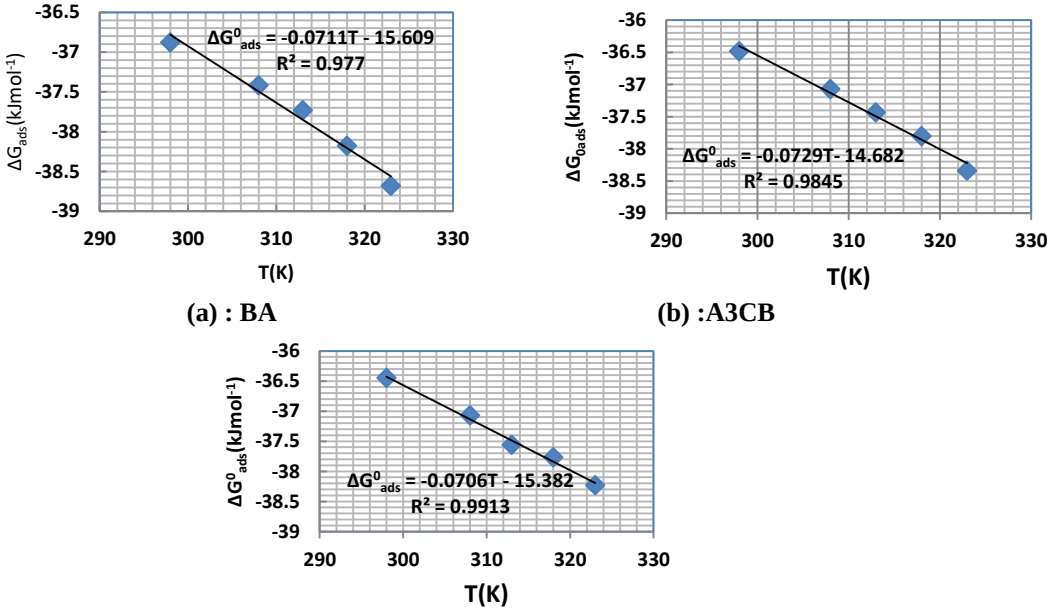

(a) : BA **(b) :A3CB**

(c) :A3PTB

Figure 4 : ΔG^0_{ads} versus temperature for the three molecules

The values of these functions are shown in Table 2

Table 2 : Adsorption thermodynamic functions of the three molecules.

Molecule	T(K)	$\Delta G^0_{ads}(kJmol^{-1})$	$\Delta H^0_{ads}(kJmol^{-1})$	$\Delta S^0_{ads}(Jmol^{-1}K^{-1})$
BA	298	-36.88	-15.61	71.10
	308	-37.42		
	313	-37.73		
	318	-38.18		
	323	-38.68		
A3CB	298	-36.48	-14.68	72.90
	308	-37.07		
	313	-37.43		
	318	-37.80		
	323	-38.34		
A3PTB	298	-36.45	-15.38	70.60
	308	-37.07		
	313	-37.56		
	318	-37.77		
	323	-38.23		

The negative values of ΔG^0_{ads} indicate that the molecules adsorbed onto the aluminium surface spontaneously. The values of ΔG^0_{ads} are less than -20kJ. mol^{-1} and up to -40kJ. mol^{-1}, indicating that the adsorption process on the metal surface [34] is a mixed adsorption (physisorption and chemisorption). Chemisorption trends to predominate because the values of ΔG^0_{ads} are closer to -40kJ. mol^{-1}, what explains that there is electron transfer from the heteroatom of the molecules to the metal surface leading to the formation of coordinate bonds.

Values of change in standard adsorption enthalpy ΔH^0_{ads} are negative, showing an exothermic adsorption process for the three molecules. In the case of change in standard adsorption entropy, the values are positive, indicating an increase in disorder due to the desorption of water molecules.

Type of adsorption

In order to elucidate the adsorption type, we used the Adejo-Ekwenchi isotherm [35] which is given by the following equation :

$$log\left(\frac{1}{1-\theta}\right) = logK_{AE} + blog\ C \qquad (20)$$

Where C is the concentration of the adsorbate, K_{AE} and b are the isotherm parameters. Figure 5 gives the obtained straight lines.

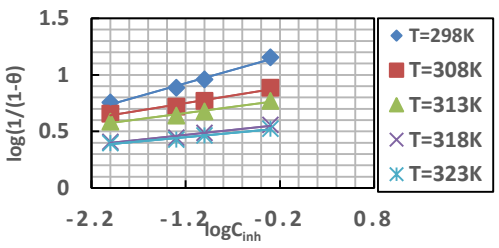

BA

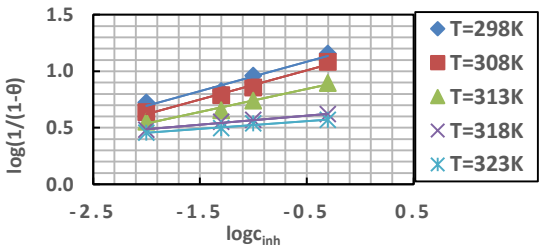

A3CB

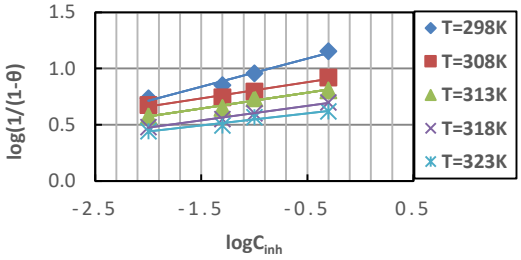

A3PTB

Figure 5 : Plots of Adejo-Ekwenchi isotherm

The obtained parameters are in Table 3.

Table 3 : Parameters of Adejo-Ekwenchi isotherm

Molecule	T(K)	R^2	b	K_{AE}
BA	298	0.9873	0.2357	16.21
	308	0.9712	0.1355	9.20
	313	0.9804	0.1091	6.22
	318	0.9623	0.0894	3.78
	323	0.9695	0.0753	3.46
A3CB	298	0.9637	0.2610	16.40
	308	0.9845	0.2592	13.75
	313	0.9839	0.2042	8.82
	318	0.9858	0.0805	4.45
	323	0.9633	0.0686	3.92
A3BTB	298	0.9791	0.2497	16.33
	308	0.9725	0.1439	8.92
	313	0.9898	0.1396	7.16
	318	0.9913	0.1291	5.40
	323	0.9517	0.1079	4.53

The Adejo-Ekwenchi isotherm [36, 37] indicates that a decrease in the value of b with rise in temperature signifies physisorption predominance, while increase or fairly constant value indicates chemisorption predominance. From Table 3, one can see that the parameters of the adsorption of the studied molecules onto the aluminium surface explain unambigously the predominance of physisorption as b decreases with rise in temperature.

Effect of the temperature

In order to evaluate the apparent energy (E_a) in the absence and in the presence of the molecules, the modified form of the Arrhenius equation [38] was used :

$$logW = logk - \frac{E_a}{2.3RT} \qquad (21)$$

Where W is the corrosion rate, k is the Arrhenius pre-exponential constant and T is the absolute temperature. The values of (E_a) were deduced from the plots of logW versus 1/T (Figure 5).

The changes in activation enthalpy (ΔH_a^*) and entropy (ΔS_a^*) [39] were determined using the transition state equation :

$$log\left(\frac{W}{T}\right) = \left[log\left(\frac{R}{\aleph h} + \frac{\Delta S_a^*}{2.303R}\right)\right] - \frac{\Delta H_a^*}{2.303RT} \qquad (22)$$

Where h is the Planck constant, R is the perfect gas constant and $\aleph$ is the Avogadro number.

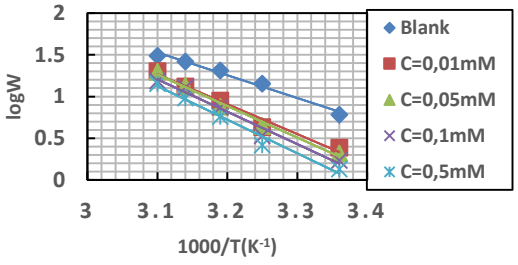

BA

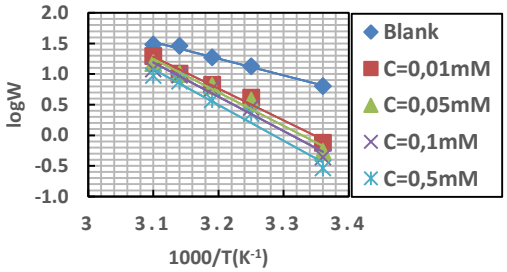

A3CB

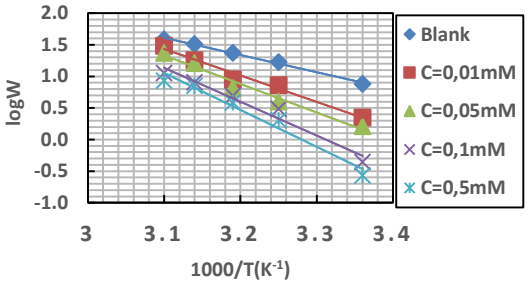

A3PTB

Figure 5 : logW versus 1/T

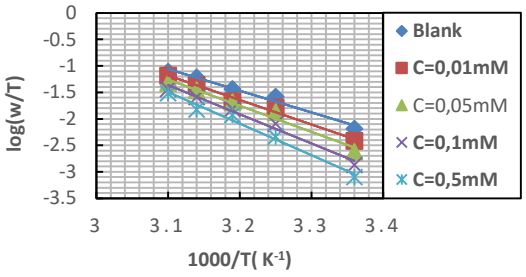

BA

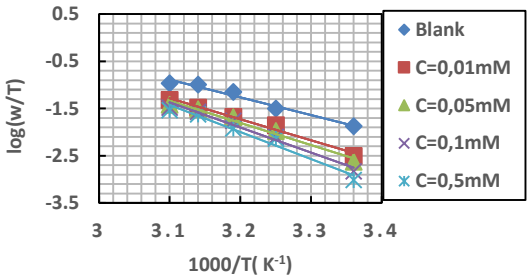

A3CB

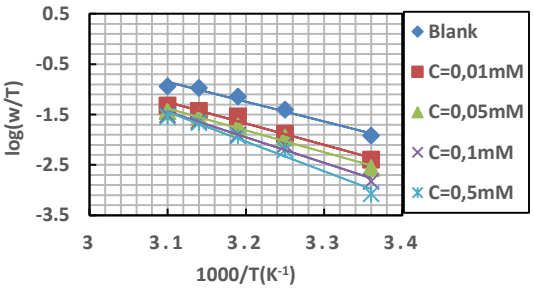

A3PTB

Figure 6 : logW versus 1/T

The plots of logW and that of $\log(\frac{W}{T})$ versus 1/T (Figures 5 and 6) lead to different parameters given in Table 4.

Table 4 : Activation parameters of the three studied molecules

Molecule	C (mol/L)	Arrhenius plots			Transition state equation		
		$logk$	$E_a(kJmol^{-1})$	R^2	ΔH_a^* (kJ/mol)	ΔS_a^* (J. mol-^{1}K^{-1})	R^2
BA	0	9.976	52.19	0.9841	78.352	24.990	0.9787
	0.01	12.378	68.62	0.9758	88.747	54.917	0.9850
	0.05	13.015	72.58	0.9759	94.493	71.269	0.9738
	0.1	13.258	74.43	0.9896	105.505	103.342	0.9819
	0.5	13.652	77.37	0.9797	114.268	128.060	0.9830
A3CB	0	9.973	52.19	0.9867	71.957	8.486	0.9720
	0.01	17.459	99.89	0.9823	85.580	48.199	0.9833
	0.05	18.243	104.96	0.9708	89.997	55.856	0.9771
	0.1	18.555	107.26	0.9724	101.675	91.335	0.9735
	0.5	19.235	112.12	0.9700	109.587	114.848	0.9684
A3PTB	0	10.06	52.19	0.9941	68.101	18.978	0.9739
	0.01	14.40	89.65	0.9771	71.572	30.122	0.9785
	0.05	15.37	91.87	0.9727	83.054	33.453	0.9826
	0.1	17.71	101.81	0.9664	97.445	76.860	0.9826
	0.5	19.19	112.12	0.9679	112.890	114.670	0.9748

According to the literature [40], the effect of temperature on the inhibition efficiency is related to the three types of inhibitors :

- Inhibitors with a decrease in inhibition effiiency with rise in temperature : E_a(uninhibited) $< E_a$ (inhibited) ;
- Inhibitors showing no changes in inhibition efficieny with increase in temperature : E_a does not change ;
- Inhibitors showing an increase in inhibition efficiency with rise in temperature : E_a(uninhibited) $> E_a$ (inhibited)

Observing our results, for all the three molecules E_a(blank) $< E_a$ (inhibited), what according to the literature [41] is attributed to the predominance of physisorption.

The positive sign of change in activation enthalpy (ΔH_a^*) reflects the endothermic nature of the aluminium dissolution process. We can see that the activation energy (E_a) increases with rise in the inhibitors concentration, showing that the aluminium dissolution becomes more and more difficult. For a given concentration,

We can see that change in activation entropy (ΔS_a^*) is positive, showing that the disorder increases on going from reactants to activated complex.

Quantum chemistry

The Gaussian 5.0 packet program [42] was used to establish the starting geometries of the studied molecules and Gaussian 09 W [43] software was used to perform the calculations. We used DFT approach [44] with B3LYP correlation functionnal [45] and the 6-311 G (d, p) basis set. Figure 6 gives the optimized representations of the molecules.

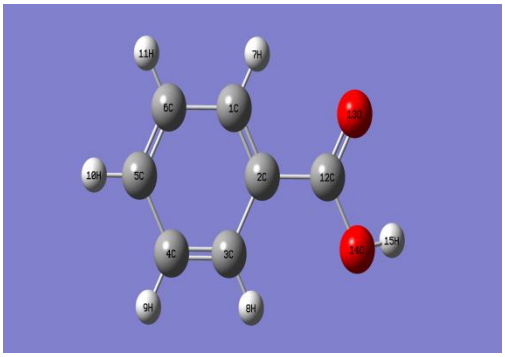

BA

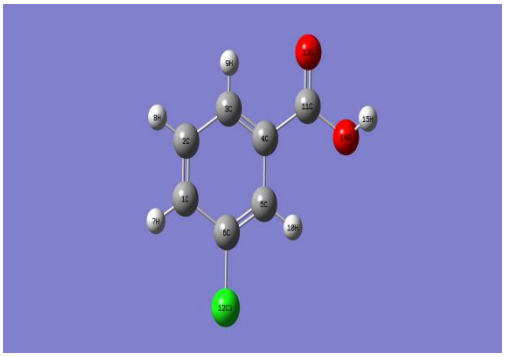

A3CB

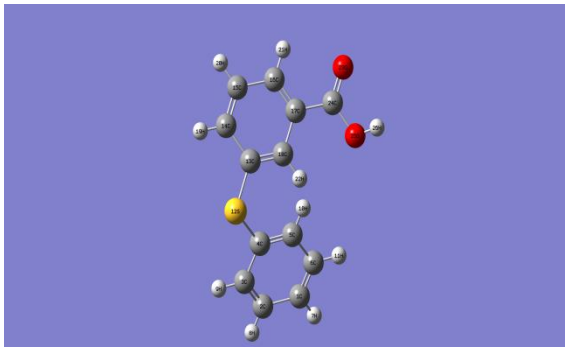

A3PTB

Figure 6 : Optimized structures of the studied molecules

Global molecular descriptors

The calculations were performed in gas phase. The quantum chemical parameters computed are given in Table 5.

The most significant parameters in Table 5 are the frontier molecular energies : the energy of the highest occupied molecular orbital (E_{HOMO}) the energy of the lowest unoccupied molecular orbital (E_{LUMO}) and the energy gap (ΔE). E_{HOMO} is related to electron donating capacity of the molecule, while E_{LUMO} [46] is related to the affinity of the molecule to accept electrons. A higher value of E_{HOMO} and a lower value of E_{LUMO} lead generally to a low energy gap [47], what leads to a good inhibition efficiency.

Table 5 : Global parameters of the studied molecules.

Parameter	DFT/ B3LYP/6-311 G (d, p)		
	BA	**A3CB**	**A3PTB**
$E_{HOMO}\ (eV)$	-7,3304	-7,2458	-6,1450
$E_{LUMO}\ (eV)$	-1,5656	-1,8942	-1,6336
Energy gap, $\Delta E\ (eV)$	5,7648	5,3516	4,5114
Dipole $\mu\ (D)$	1,9607	0,4013	2,0468
Ionisation Energy $(I(eV)$	7,3304	7,2458	6,1450
Electronic Affinity $A(eV)$	1,5656	1,8942	1,6336
Electronegativity$\chi\ (eV)$	4,449	4,5700	3,8893
Global hardness $\eta\ (eV)$	2,8824	2,6758	2,2557
Global Softness $\sigma(eV)^{-1}$	0,3469	0,3737	0,4433
Fraction of electrons tranferred ΔN	-0,0293	-0,0542	0,0866
Electrophylicity index ω	3,4335	4,7565	3,3523
Total Energy E_T(Ha)	-420.9	-880.6	-1050.2

The other global molecular descriptors derive from the frontier molecular energies. Although the dipole moment μ is used to predict the direction of a corrosion process, the literature [48] is inconsistent on its contribution to identify a good or bad corrosion inhibitor.

Global hardness (η) and global softness (σ) are other parameters that give information on the inhibition efficiency of a molecule. A hard molecule has a high energy gap whereas a soft molecule has a low energy gap. So, the molecule with least value of global hardness (high value of softness) [49] is considered as a good corrosion inhibitor, what is in agreement with our results (BA : $\eta = 2.8824\ eV, \sigma = 0.3469$; A3CB : $\eta = 2.6758 eV, \sigma = 0.0.3737$ and A3PTB :$\eta = 2.2557\ eV, \sigma = 0.4433$).

The electronegativity (χ) [50] measures the power of an atom or group of atoms to attract electrons. The calculated values (Table 5) reveal that A3CB has the highest capacity to attract electrons ($\chi_{A3CB} > \chi_{BA} > \chi_{A3PTB}$).

Two other important parameters are the fraction of electrons transferred (ΔN) and the electrophylicity index (ω). (ΔN) [51] expresses the tendency of a molecule to give electrons to the metal whereas (ω) [52] shows the capacity of the molecule to accept electrons from the metal. In our work, the values of (ΔN) (-0.0293 ; -0.0542 ; 0.0866 respectively for BA, A3CB and A3PTB) and that of (ω) (3.4335 ; 4.7565 ; 3.3523 respectively for BA, A3CB and A3PTB) reveal the tendency of BA and A3CB to receive electrons from the metal, while A3PTB can give electrons to the metal or receive electrons from it.

Local descriptors

The Fukui functions f_k^+ and f_k^- and the dual descriptor $\Delta f_k(r)$ provide more informations about the reactivity of the investigated molecules. They help [53-55] to access to the reactivity of each atomic center of a molecule : f_k^+ is associated to the reactivity for nuleophilic attack ; it measures [56-58] the intramolecular reactivity at the site towards a nucleophilic reagent, while f_k^- is associated to the reactivity for electrophilic attack ; it measures the intramolecular reactivity at the site r towards an electrophilic reagent. According to the literature [59, 60], the dual descriptor is more efficient in predicting the reactive sites of a molecule than the Fukui functions. Table 6 gives the reactive sites of the studied molecules.

Table 6 : Nucleophilic and electrophilic sites in the studied molecules.

Molecule	Atom	$q_k(N+1)$	$q_k(N)$	$q_k(N-1)$	f_k^+	f_k^-	Δf_k
BA	**C(2)**	0.112687	-0.022637	0.169698	**0.339057**	**-0.396068**	**0.735125**
	C(12)	-0.033942	0.425574	0.164245	**-0.459516**	**0.261329**	**-0.720845**
A3CB	**C(11)**	-0.022257	0.4309	0.203156	**-0.453157**	**0.227744**	**-0.680901**
	O(15)	0.062985	-0.333822	0.155882	**0.396807**	**-0.489704**	**0.886511**
A3PTB	**O(23)**	0.004053	-0.338543	0.108264	**0.342596**	**-0.438807**	**0.781403**
	C(24)	0.001179	0.427608	0.125442	**-0.426429**	**0.302166**	**-0.728595**

According to the literature [61] the process is driven by a nucleophilic attack on atom k when $\Delta f_k > 0$ and atom k acts as an electrophilic species. In the inverse case,$\Delta f_k < 0$, the process is driven by an electrophilic attack on atom k which acts as a nucleophilic species.

In Table 6, one can see that :

- C(12), C(11) and C(24) are respectively the electrophilic attack centers of BA, A3CB and A3PTB ;
- C(2), O(15) and O(23) are respectively the nucleophilic attack centers of BA, A3CB and A3PTB.

The HOMO and LUMO orbitals that illustrate the Fukui and dual functions are given by Figure 7.

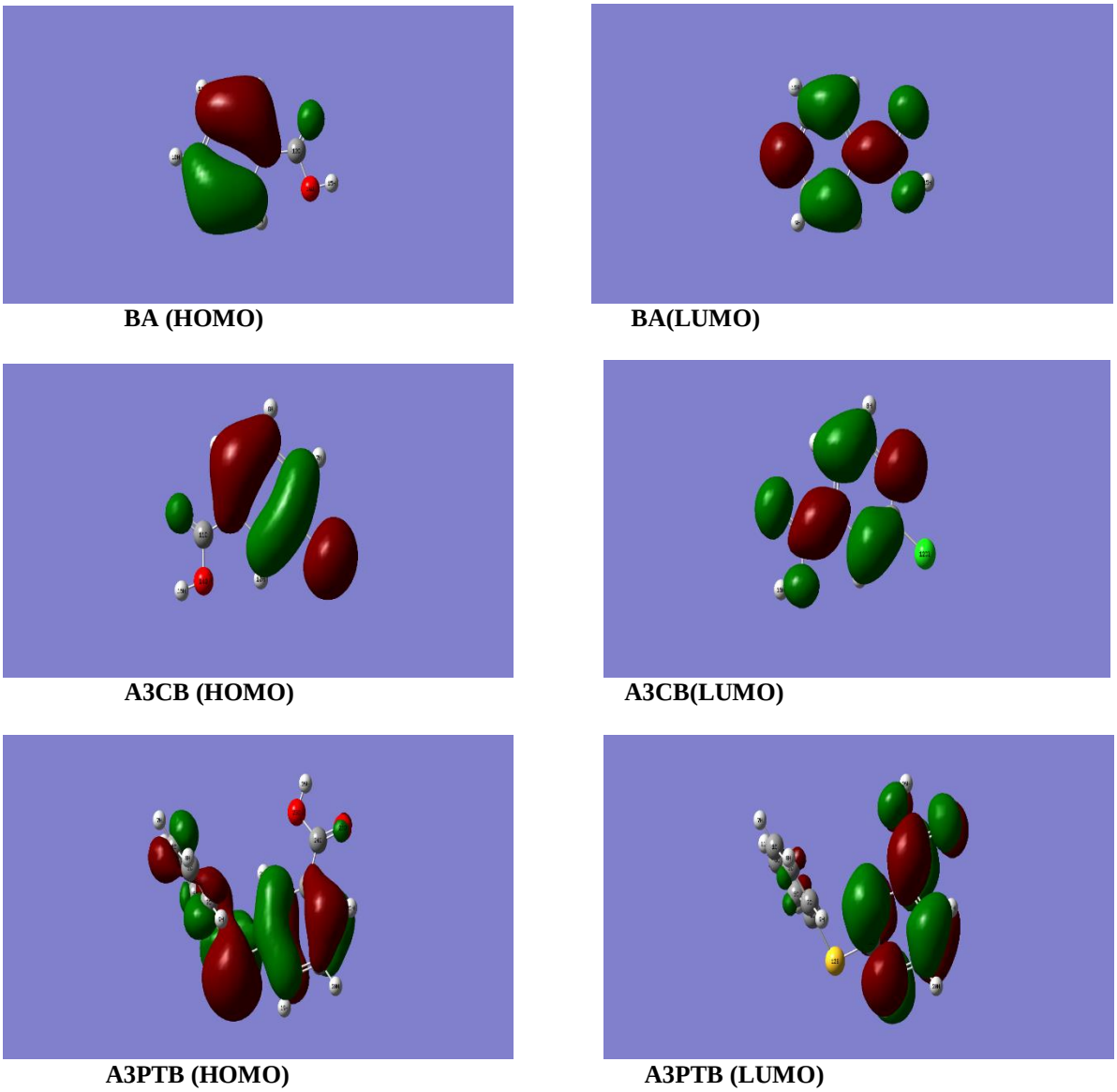

BA (HOMO) **BA(LUMO)**

A3CB (HOMO) **A3CB(LUMO)**

A3PTB (HOMO) **A3PTB (LUMO)**

Figure 7 : HOMO and LUMO orbitals for the investigated molecules (BA, A3CB and A3PTB)

PCA and QSPR studies

PCA is a statistical method used to convert multivariate data sets into a few comprehensive data by maintaining a large amount of information from the original data. Many techniques have been developed for this purpose but Principal Component Analysis (PCA) [62-64] is one of the oldest and the most used method in many disciplines. In sum, the objective of PCA is to reduce the number of variables of a data set while preserving as much information as possible. The procedure to access to principal component includes three steps :

- Calculating the multivariate correlation matrix from the simple data ;
- Computing eigen values and eigen vectors of the correlation matrix ;
- Generating the PCs ; each PC is a linear combination of optimally weigh original variable, such as :

$$P_i = b_{i1}X_1 + b_{i2}X_2 + \cdots + b_{ik}X_k \qquad (23)$$

In our case, the correlation matrix obtained is given below.

	EI(%)	**ΔE**	**V_m**	**LogP**	**E_{HOMO}**	**E_{LUMO}**	**μ**
EI(%)	1						
ΔE	**-0.99021667**	1					
V_m	0.46148	-0.36339333	1				
LogP	**0.98990667**	-0.99999667	0.36179667	1			
E_{HOMO}	**0.92387667**	-0.96824	0.16973267	0.96878333	1		
E_{LUMO}	0.84674	-0.91269	0.03400967	0.91358333	0.98587667	1	
μ	0.88870333	-0.94398333	0.10267633	0.94470667	0.99651	0.99641667	1

The values of LogP and V_m are from Molinspiration software (**BA** : miLogP = 1.85 and V_m = 111.05Å^3 ; **A3CB** : miLogP = 2. 50 and V_m = 124.58 Å^3 ; **A3PTB** : miLogP = 3.81 and V_m = 200.58Å^3).

To establish the mathematical relationship (linear model, equation (15)) between the inhibition efficiency and the molecular descriptors, we have constructed sets of three descriptors by association of one highly ($\Delta E, logP, E_{HOMO}$) and two much less (V_m, μ, E_{LUMO}) corraleted to the inhibition efficiency. The objective of our work is to minimize the difference between experimental and predicted values of inhibition efficiency. In this context, the constituted sets are : ($\Delta E, E_{LUMO}, \mu$), (LogP, E_{LUMO}, μ), (E_{HOMO}, E_{LUMO}, μ).

The values of the coefficients (A, B and D) for the three sets are in Tables 7.

Table 7 : Coefficients of the linear model established with the three descriptors sets

C(M)	($\Delta E, E_{LUMO}, \mu$)			(LogP, E_{LUMO}, μ)			(E_{HOMO}, E_{LUMO}, μ)		
	A	B	D	A	B	D	A	B	D
10^{-5}	-5.6	-56.3	10.9	2.7	-37.7	7.6	-3.8	-26.8	7.4
5.10^{-5}	-5.4	-58.1	10.1	2.6	-39.9	6.9	-3.7	-29.2	6.7
10^{-4}	-3.7	-55.4	9.9	1.8	-43.0	7.7	-2.5	-35.7	7.5
5.10^{-4}	-7.2	-67.0	12.1	3.5	-43.0	7.8	-4.9	-28.9	7.5

Figure 8 represents IE_{theo}(%) versus IE_{exp}(%)

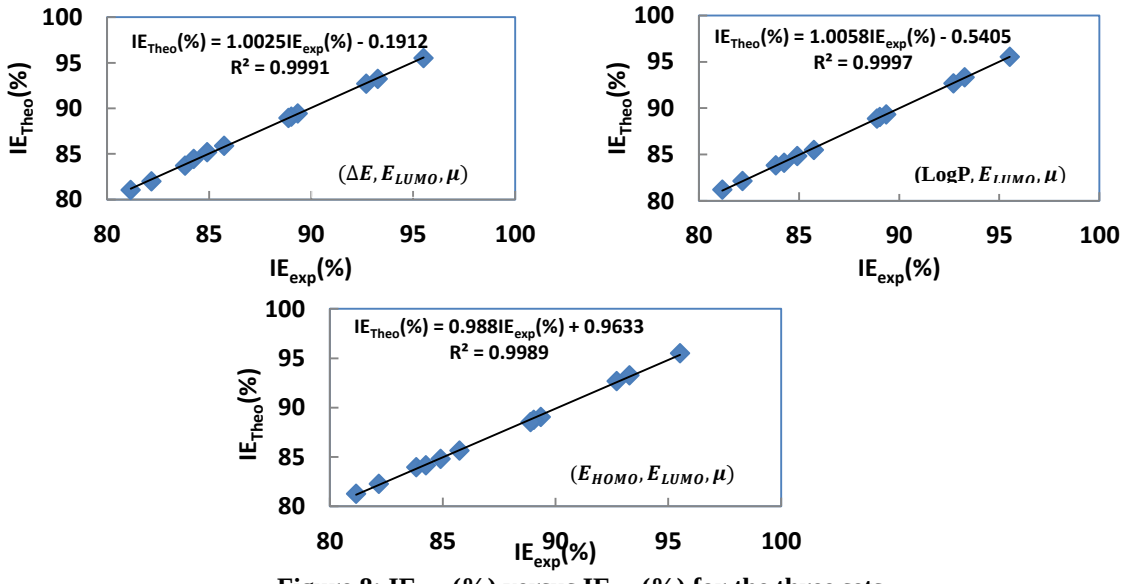

Figure 8: IE_{theo} (%) versus IE_{exp} (%) for the three sets

In order to determine the best set in each type of models, we use the following statistical criteria :

- R^2 (détermination coefficient) : $R^2 = 1 - \frac{\sum_{i=1}^{N}\left(IE_{exp}^{i} - IE_{theo}^{i}\right)^2}{\sum_{i=1}^{N}\left(IE_{i}^{exp} - IE_{theo}^{i}\right)^2}$ (24)

- RMSE (Root Mean Squared Error) : $RMSE = \sqrt{\sum_{i=1}^{N} \frac{\left(IE_{exp}^{i} - IE_{theo}^{i}\right)^2}{N-1}}$ (25)
- MPD (Mean Percent Deviation) : $\frac{1}{N}\sum_{i=1}^{N}\left|\frac{IE_{exp}^{i} - IE_{theo}^{i}}{IE_{exp}^{i}}\right|$ (26)

The values of the statistical parameters are listed in Table 8.

Table 8 : Statistical parameters of the three studied sets

	$(\Delta E, E_{LUMO}, \mu)$			**(LogP, E_{LUMO}, μ)**			$(E_{HOMO}, E_{LUMO}, \mu)$		
Parameter	R^2	RMSE	MPD	R^2	RMSE	MPD	R^2	RMSE	MPD
Value	0.9991	0.1417	0.0013	**0.9997**	**0.0902**	**0.0004**	0.9989	0.1860	0.0016

The coefficient of determination (R^2) measures how well a statistical model predicts an outcome. The lowest possible value of (R^2) is 0 and the highest possible value is 1. When (R^2) is high (near 1), the observations are lose to the model's prediction.

RMSE is a metric that tells us the average distance between the predicted values from the model and the values in the dataset. The lower the RMSE, better a given model is able to fit dataset.

MPD measures the degree to which individual data points in a statistic deviate from the average measurement of that statistic.

Observing the values of the parameters inTable 8, one can see that the best set is (LogP, E_{LUMO}, μ) with determination coefficient (R^2 = 0.9997), Root Mean Square Error (RMSE = 0.0902) and Mean Percent Deviation (MPD = 0.004).

Principal Component Analysis (PCA) [65] is used to transforme a large set variables into a smaller one that still contains most in the information of the large set. To access to principal components, we used the correlation matrix which allows us determining the eigenvectors and the eigenvalues :

- $(\mathbf{\Delta E, E_{LUMO}, \mu})$

	ΔE	E_{LUMO}	μ
ΔE	1	-0.98629333	-0.24202567
E_{LUMO}	-0.98629333	1	0.31329667
μ	-0.24202567	0.31329667	1

The related eigenvalues and eigenvetors are given below :

$$\boldsymbol{\lambda_{1=2.95342}} \qquad \vec{V}_1 \begin{pmatrix} \mathbf{-0.572706} \\ \mathbf{0.579659} \\ \mathbf{0.579659} \end{pmatrix}$$

$$\boldsymbol{\lambda_{2=0.0465819}} \qquad \vec{V}_2 \begin{pmatrix} \mathbf{-0.819761} \\ \mathbf{-0.404964} \\ \mathbf{-0.404964} \end{pmatrix}$$

- $\mathbf{(LogP, E_{LUMO}, \mu)}$

	LogP	E_{LUMO}	μ
LogP	1	0.37955667	0.116659
E_{LUMO}	0.37955667	1	0.96313
μ	0.116659	0.96313	1

The eigenvalues and eigenvectors are :

$$\boldsymbol{\lambda_{1=2.07904}} \qquad \vec{V}_1 \begin{pmatrix} \mathbf{0.313554} \\ \mathbf{0.691327} \\ \mathbf{0.650962} \end{pmatrix}$$

$$\boldsymbol{\lambda_{2=0.920956}} \qquad \vec{V}_2 \begin{pmatrix} \mathbf{-0.929452} \\ \mathbf{0.6830783} \\ \mathbf{0.359467} \end{pmatrix}$$

- $\mathbf{(E_{HOMO}, E_{LUMO}, \mu)}$

E_{HOMO} E_{LUMO} μ

E_{HOMO}	1	0.25929833	-0.72427333
E_{LUMO}	0.25929833	1	-0.35916
μ	-0.72427333	-0.35916	1

Corresponding eigenvalues and eigenvectors are :

$$\lambda_{1=1.93048} \qquad \vec{V}_1 \begin{pmatrix} -0.626601 \\ -0.426415 \\ 0.652335 \end{pmatrix}$$

$$\lambda_{2=0.80209} \qquad \vec{V}_1 \begin{pmatrix} 0.385868 \\ -0.896986 \\ -0.215692 \end{pmatrix}$$

The percentage of information for each eigenvalue is given by :

$$P_i = \frac{\lambda_i}{\sum_{i=1}^{n} \lambda_i} \qquad (27)$$

Table 9 resumes the values of percentage information for eigenvalues for the three sets.

Table 9 : Percentage of information for each eigenvalue in each set.

Set	P_1(%)	P_2(%)
$(\Delta E, E_{LUMO}, \mu)$	98.6	1.4
$(LogP, E_{LUMO}, \mu)$	69.3	30.7
$(E_{HOMO}, E_{LUMO}, \mu)$	70.6	29.4

Observing Table 9, one can see that in the case of $(\Delta E, E_{LUMO}, \mu)$, all the information is given by ΔE ; soi t is possible to establish a model containing only one parameter by representing IE(%) versus ΔE (Figure 9) for the highest inhibitors concentration.

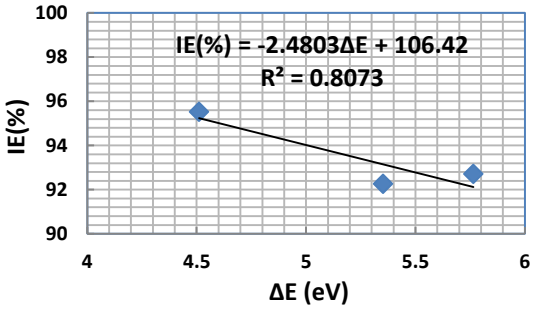

Figure 9 : IE(%) versus ΔE

The equation of the model confirms that IE(%) decreases when ΔE increases.

For the two other sets, we can't neglected the second eigenvalue ; so, we considered two parameters : $(LogP, E_{LUMO})$ and (E_{HOMO}, E_{LUMO}).

To establish the model, we considered a topological parameter nt_{rob} (from Molinspiration) which measures the molecular flexibility and which has not great influence on the inhibitor performance.

Table 10 gives the coefficients of the two models (IE_{Theo}(%) = Ax_i+Bxj+Res).

Set C(M)	$(LogP, E_{LUMO})$			(E_{HOMO}, E_{LUMO})		
	A	B	D	A	B	D
10^{-5}	-26.69	-62.70	29.12	58.86	-244.74	44.03
5.10^{-5}	-24.10	-62.65	26.49	53.14	-227.02	39.96
10^{-4}	-27.85	-68.25	29.39	61.42	-258.22	44.95
5.10^{-4}	-26.67	-68.66	29.87	58.80	-250.53	44.77

In the equation, Res = nrotb*D.

Figure 10 represents $IE_{Theo}(\%)$ versus $IE_{Exp}(\%)$ for the two new sets $(LogP, E_{LUMO})$ and (E_{HOMO}, E_{LUMO}).

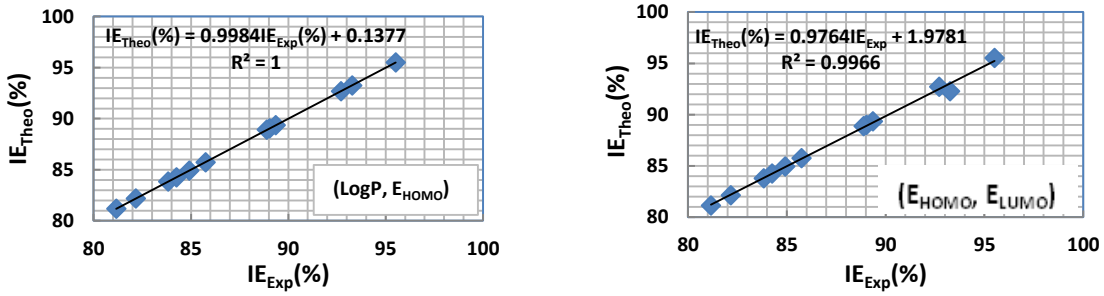

Figure 10 : $IE_{Theo}(\%)$ versus $IE_{Exp}(\%)$ for the models with two parameters

IV. Conclusion

The investigated molecules have good inhibition efficiencies for aluminium corrosion in 1M hydrochloric acid. The adsorption thermodynamic functions showed that the adsorption is spontaneous and exothermic. The adsorption isotherms showed that the adsorption is composed of physisorption and chemisorption with a predominance of physisorption. The activation functions showed endothermic dissolution with an increase disorder from reactants to activated complexes. The quantum chemical parameters confirmed the good inhibitors characters of the studied molecules, and they indicated the probable sites of interactions with the metal. The use of PCA reduced the number of parameters and helped in the choice of the pertinent descriptors for the sets used in the QSPR models.

References

[1]. C. Vargel, Corrosion of Aluminium, 1st éd ; Elsevier : Amsterdam ; Boston, 2004.
[2]. B. R. Strohmeier, an ESCA method for determining the oxide thickness on aluminium alloys, Surf. Interface Anal, 15, 51-56, 1990.
[3]. A. A. El-Hosary, R. M. Saleh, Progressin understanding and prevention of corrosion, Institut of Materials ; *London* 2 : 911-920, 1993.
[4]. A. Handy, N. Sh El-gendy, Thermodynamic, Adsorption and electrochemical studies for corrosion inhibition of carbon steel by hanna extract in acid medium Egypt. *J. Petrol.* 22: 17-25. 2013
[5]. B. Muralidharam, B. Hammouts, N. Lagrenee, F. Bentiss, Electrochemistry of Corrosion, *Science 48: 2831 – 2842.*1995
[6]. S. A. Jadhav, Self-Assembled Monolayers (SAMs) of Carboxylic Acids : Overview, Cent. Eur. J. Chem., 9(3), 369-378, 2011.
[7]. A. Ulman, Formation and Structure of Self-Assembled Monolayers, Chem. Rev., 96(4), 1533-1554, 1996.
[8]. A. A. Khadom, A. S. Yaro, and A. A. H. Kadum, Corrosion inhibition by naphthylamine and phenylenediamine for the corrosion of copper-nickel alloy in hydrochloric acid, Journal of the Taiwan Institute of Chemical Engineers, vol. 41(1) : 122–125, 2010.
[9]. A. Y. Musa, A. A. Khadom, A. A. H. Kadhum, A. B. Mohamad, and M. S. Takriff, Kinetic behavior of mild steel corrosion inhibition by 4-amino-5-phenyl-4H-1, 2, 4-trizole-3-thiol," *Journal of the Taiwan Institute of Chemical Engineers*, vol. 41(1) : 126–128, 2010.
[10]. A. Rahim and J. Kassim, "Recent Development of Vegetal Tannins in Corrosion Protection of Iron and Steel, Recent Patents on Materials Sciencee, vol. 1(3) : 223–231, 2008.
[11]. P. Greelings, F. De Proft, W. Langenaeker, Conceptual density functional theory, Chemical Reviews, 103 : 1793-1873, 2003.
[12]. M. J. Frisch, G. W. Trucks, H. B. Schlegel, G. E. Scuseria, M. A. Robb, J. R. Cheeseman, G. Scalmani, V. Barone, G. A. Petersson, H. Nakatsuji, X. Li, M. Caricato, A. V. Marenich, J. Bloino, B. G. Janesko, R. Gomperts, B. Mennucci, H. P. Hratchian, J. V. Ortiz, A. F. Izmaylov, J. L. Sonnenberg, D. WilliamsYoung, F. Ding, F. Lipparini, F. Egidi, J. Goings, B. Peng, A. Petrone, T. Henderson, D. Ranasinghe, V. G. Zakrzewski, J. Gao, N. Rega, G. Zheng, W. Liang, M. Hada, M. Ehara, K. Toyota, R. Fukuda, J. Hasegawa, M. Ishida, T. Nakajima, Y. Honda, O. Kitao, H. Nakai, T. Vreven, K. Throssell, J. A. Montgomery, Jr., J. E. Peralta, F. Ogliaro, M. J. Bearpark, J. J. Heyd, E. N. Brothers, K. N. Kudin, V. N. Staroverov, T. A. Keith, R. Kobayashi, J. Normand, K. Raghavachari, A. P. Rendell, J. C. Burant, S. S. Iyengar, J. Tomasi, M. Cossi, J. M. Millam, M. Klene, C. Adamo, R. Cammi, J. W. Ochterski, R. L. Martin, K. Morokuma, O. Farkas, J. B. Foresman, D. J. Fox, Gaussian 16 Revision A.03, 2016. Gaussian Inc. Wallingford CT.
[13]. A. D. Becke, Density-functional thermochemistry. III. The role of exact exchange, J. Chem. Phys. 98 : 5648–5652, 1993.
[14]. R. Krishnan, J. S. Binkley, R. Seeger, J. A. Pople, Self-consistent molecular orbital methods XX. A basis set for correlated wave functions, J. Chem. Phys., 72, 650, 1980.
[15]. R. G. Parr, R. A. Donelly, M. Levy, W. E. Palke, Electronegativity. The Density functional viewpoint, J. Chem. Phys., 68 : 3801, 1978.
[16]. T. Koopmans, Uber die Zuordnung von Wellenfunktionen und Eigenwerten zu den Einzelnen Elektronen Eines Atoms, Physica A: Statistical Mechanics and its Applications, vol. 1(1–6) : 104–113, 1934.
[17]. R. G. Pearson, Absolute electronegativity and hardness : application to inorganic chemistry, Inorg. Chem. 27, 734, 1988.
[18]. R. G. Parr, R.G. Pearson, Absolute hardness : companion parameter to absolute electronegativity, J. Am. Chem. Soc. 105 : 7512-7516, 1983.
[19]. G. Gece, The use of quantum chemical methods in corrosion inhibition studies, Corrosion Science, 50 : 2981-2992, 2008.
[20]. R. G. Pearson, Hard and soft acids ans bases, the evolution of a chemical concept, Coordination Chemistry Reviews, Vol. 100 (C) : 403-425, 1990.
[21]. A. Kokalj and N. Kova˘cevi´c, On the consistent use of electrophilicity index and HSAB-based electron transfer and its associated change of energy parameters, Chemical Physics Letters, vol. 507 (1-3) : 181–184, 2011.
[22]. Zarrouk, A. *et al*. A theoretical investigation on the corrosion inhibition of copper by quinoxaline derivatives in nitric acid. Int. J. Electrochem. Sci. 7 :6353–6364, 2012.
[23]. R. G. Parr, L. V. Szentp´aly, and S. Liu, Electrophilicity index, Journal of the American Chemical Society, vol. 121(9) : 1922–1924, 1999.

[24]. K. Fukui, Role of frontier orbitals in chemical reactions, Science, vol. 218(4574) : 747–754, 1982.
[25]. W. Yang, R. Parr, R. Pucci, Electron density Kohn-Sham frontier orbitals and Fukui functions. J. Chem. Phys. 81 : 2862-2863, 1984.
[26]. W. Yang and W. J. Mortier, The use of global and local molecular parameters for the analysis of the gas-phase basicity of amines, Journal of the American Chemical Society, vol. 108(19) : 5708–5711, 1986.
[27]. C. Morell, A. Hocquet, A. Grand, B. Jamart-Grégoire, A conceptual DFT study of hydrozinopeptides : assessment of nucleophilicity of nitrogen atoms by means of the dual descriptors $\Delta f(r)$, J. Mol. Struct. Theochem, 849 : 46-51, 2007.
[28]. C. Morell, A. Grand, A. Toro-Labbé, Theoretical support for using the $\Delta f(r)$ descriptor, Chem. Phys. Lett., 425 : 342-346, 2016.
[29]. M. Ringner, What is principal component analysis ?, Nat. Biotechnol. 26 : 303-304, 2008.
[30]. E. J. Candès, X. Li, Y. Ma, J. Wright, Robust principal component analysis, J. ACM 58(11) : 1-37, 2011.
[31]. H. Abdi, L. J. Williams, principal component analysis. Statistics & Data mining series, John Willey & sons, Vol.2 : 433-459, 2010.
[32]. S. M. Shaban, I. Aiad, M. M. El-Sukkary, E. A. Soliman and M. Y. El-Awady, Inhibition of mild steel corrosion in acidic medium by vanillin cationic surfactants, J. Mol. Liq. : 203, 20–28, 2015.
[33]. S. M. Shaban, I. Aiad, A. H. Moustafa and O. H. Aljoboury, Some alginates polymeric cationic surfactants ; surface study and their evaluation as biocide and corrosion inhibitors, J. Mol. Liq. 273 : 164–176, 2019.
[34]. A. A. Abdulridha, M. A. Albo Hay Allah, S. Q. Makki, Y. Sert, H. E. Salman and A. A. Balakit, Corrosion inhibition of carbon steel in 1M H_2SO_4 using new azo-schiff compound : Electrochemical, gravimetric, adsorption, surface and DFT studies, J. Mol. Liq., Vol. 315 : 1-29, 2020.
[35]. S. O. Adejo, M. M. Ekwenchi, Proposing a new empirical adsorption isotherm known as Adejo-Ekwenchi isotherm, IOSR Journal of Applied Chemistry (IOSR-JAC), Vol. 6 (5) : 66-71, 2014.
[36]. S.O. Adejo, M. M. Ekwenchi, J. U. Ahile, J. A. Gbertyo, A. Kaior, Resolution of Adsorption Characterisation Ambiguity through the Adejo-Ekwenchi Adsorption Isotherm: A Case Study of Leaf Extract of Hyptis suaveolens Poit as Green Corrosion Inhibitor of Corrosion of Mild Steel in 2 M HCl, J. Emerging Trends in Eng. Appl. Sci., 5 : 201-205, 2014.
[37]. S.O. Adejo, M. M. Ekwenchi, P. O. Olatunde, F. Agbajeola, Adsorption characteristics of ethanol root extract of Portulaca oleracea as eco-friendly inhibitor of corrosion of mild steel in H_2SO_4 medium IOSR J. Appl. Chemisrty, 7 : 55-60, 2014.
[38]. M.M. Solomon, S.A. Umoren, I.I. Udousoro, A.P. Udoh, Inhibition and adsorption behaviour of carboxymethl cellulose on mild steel corrosion in sulphuric acid solution, Corros. Sci. 52 : 1317-1325, 2010.
[39]. E.E. Ebenso, Synergistic effect of halide ions on the corrosion of aluminium in H_2SO_4 using 2-acetylphenothiazine, Mater. Chem. Phys. 79 : 58-70, 2003.
[40]. S. A. Umoren, I. B. Obot, L. E. Apkabio, S. E. Etuk, Adsorption and corrosive inhibitive properties of Vigna unguiculata in alkaline and acidic media, Pigment & Resin Technology. 37(2): 98-105, 2008.
[41]. Dehri I, Ozcan M, Investigation of adsorption of isoniazid derivatives at mild steel/ hydrochloric acid interface : Electrochemical and weight loss methods, Mater Chem. Phys., 123 : 666-677, 2010.
[42]. E. Frisch, H.P. Hratchian, R.D. Dennington II et al., Gaussview, Version 5.0.8, 235 Gaussian Inc., Wallingford, CT, 2009.
[43]. J. Foresman, E. Frish, Exploring chemistry, Gaussian Inc., Pittsburg, USA, 1996.
[44]. N. O. Eddy, H. Momoh-Yahaya, and E. E. Oguzie, Theoretical and experimental studies on the corrosion inhibition potentials of some purines for aluminum in 0.1 M HCl, Journal of Advanced Research, 6 : 203–217, 2015.
[45]. N. O. Eddy, Experimental and theoretical studies on some amino acids and their potential activity as inhibitors for the corrosion of mild steel, part 2, Journal of Advanced Research, 2 : 35–47, 2011.
[46]. Khalil N., Quantum Chemical Approach of corrosion inhibition, Electrochim. Acta. 48 : 2635-2640, 2003.
[47]. R. Karthikaiselvi, S. Subhashini, Study of adsorption properties and inhibition of mild steel corrosion in hydrochloric acid media by water-soluble composite poly (vinyl alcohol-o-methoxy aniline). J. Assoc. Arab Univ. Basic Appl. Sci. 16 : 74–82, 2014.
[48]. G. Gece, The use of quantum chemical methods in corrosion inhibitor studies, Corros. Sci. 50(11) : 2981-2992, 2008.
[49]. E. E. Ebenso, D. A. Isabirye, N. O. Eddy, Adsorption and Quantum Chemical Studies on the Inhibition Potentials of Some Thiosemicarbazides for the Corrosion of Mild Steel in Acidic Medium, Int. J. Mol. Sci. 11 : 2473-2498, 2010.
[50]. I. Ahamad, R. Prasad, M. A. Quraishi, Adsorption and inhibitive properties of some new Mannich bases of isatin derivatives on corrosion of MS in acidic media, Corros. Sci. 52, 1472-1481, 2010.
[51]. K. Benbouguerra, S. Chafaa, N. Chafai and M. Mehri, Synthesis, spectroscopic characterization and a comparative study of the corrosion inhibitive efficiency of an α-aminophosphonate and Schiff base derivatives: Experimental and theoretical investigations J. Mol. Struct. 1157 : 165-176, 2018.
[52]. J. Saranya, P. Sounthari, K. Parameswari, and S.Chitra, Adsorption and density functional theory on corrosion ofmild steel by a quinoxaline derivative, Der Pharma Chemica, vol. 7(8) : 187–196, 2015.